Role of Crack Size and Microstructure in Influencing Mixed-Mode High-Cycle Fatigue Thresholds in Ti-6Al-4V

R. K. Nalla and R. O. Ritchie[1]

Department of Materials Science and Engineering, University of California, Berkeley, CA 94720-1760

ABSTRACT

High-cycle fatigue of turbine components remains a principal cause of failures in military aircraft engines. One critical issue involves the fatigue threshold under multiaxial loading conditions. To address this, the effect of microstructure on mixed-mode (mode I+II) high-cycle fatigue thresholds in a Ti-6Al-4V turbine engine alloy is investigated for crack sizes ranging from a few microns to several millimeters. Thresholds were determined for both fine-grained bimodal and coarse lamellar microstructures, under pure mode I ($\Delta K_{II}/\Delta K_I = 0$) to nearly pure mode II ($\Delta K_{II}/\Delta K_I \sim 7.1$) conditions, at load ratios (minimum load/maximum load) from 0.1 to 0.8. Thresholds were characterized in terms of the strain-energy release rate, incorporating both tensile and shear loading components. In the presence of large (>4 mm) through-thickness cracks, significant effects of mode-mixity and load ratio were observed, with the lamellar alloy displaying the superior resistance. These effects were markedly reduced when crack-tip shielding was accounted for. Furthermore, when thresholds were measured for cracks comparable in size to microstructural dimensions, i.e., for through-thickness short (~200 μm) cracks and microstructurally-small (<50 μm) surface cracks, such effects were similarly reduced.

Keywords high-cycle fatigue; mixed mode; fatigue thresholds; load ratio; short cracks.

INTRODUCTION

The control of failures resulting from high cycle fatigue (HCF) in turbine engine components has been identified as one of the major challenges facing the readiness of the U.S Air Force fleet [e.g., 1]. A critical issue involves the effects of mixed-mode (tensile and shear) loads on such failures, conditions that are known to exist in many fatigue-critical locations within the engine, e.g., where fretting cracks form in the blade/dovetail contact section [2]. The effective crack-driving force can be defined here as a combination of the tensile, mode I, ΔK_I, in-plane shear, mode II, ΔK_{II}, and/or anti-plane shear, mode III, ΔK_{III}, stress-intensity ranges. From the purpose of failure prevention, it is critical that fatigue-crack growth thresholds are well characterized for such loading, as the extremely high frequencies (~1-2 kHz) can lead to rapid failures. To date, most studies on the HCF performance of engine alloys have focused on a bimodal microstructure of Ti-6Al-4V, an α+β alloy used in fan disks and compressors in the front, low-temperature, stages of the engine [e.g., 3-8]. In this work, we extend these earlier observations to a fully lamellar microstructure. Furthermore, the role of crack size is also investigated through the study of large (> 4 mm) and short (~200 μm) through-thickness cracks and microstructurally-small (<50 μm) surface cracks, over a range of mode-mixities, from pure tension to predominantly shear ($\Delta K_{II}/\Delta K_I \sim$ 0 to 7.1), at load ratios (ratio of minimum to maximum load) from $R = 0.1$ to 0.8.

[1] Corresponding author: Tel: (510) 486-5798; Fax: (510) 486-4881.
E-mail address: roritchie@lbl.gov (R. O. Ritchie).

MATERIALS AND EXPERIMENTAL PROCEDURES

The material investigated was a Ti-6Al-4V alloy, of composition (in wt.%) 6.3 Al, 4.17 V, 0.19 Fe, 0.19 O, 0.013 N, 0.0041 H, bal. Ti. The alloy originated as bar stock and was produced by Teledyne Titanium (Pittsburgh, PA). The as-received microstructure was in the bimodal condition (also termed solution-treated-and-overaged), and consisted of colonies of equiaxed primary-α and lamellar $\alpha+\beta$ (transformed-β), with an average grain size of ~20 μm, (Fig. 1a). This was compared to a lamellar microstructure, obtained by solution treating *in vacuo* at 1005°C (just above the β-transus) for ~30 min, quenching at ~100°C/min in helium and stabilizing 2 hr at 700°C *in vacuo*. The resulting Widmanstätten structure (Fig. 1b) had an average prior-β grain size of ~1 mm, a colony size of ~500 μm. Mechanical properties (for the L-orientation using strain rates of 5 x 10^{-4} s^{-1}) are listed in Table I (see also [9].

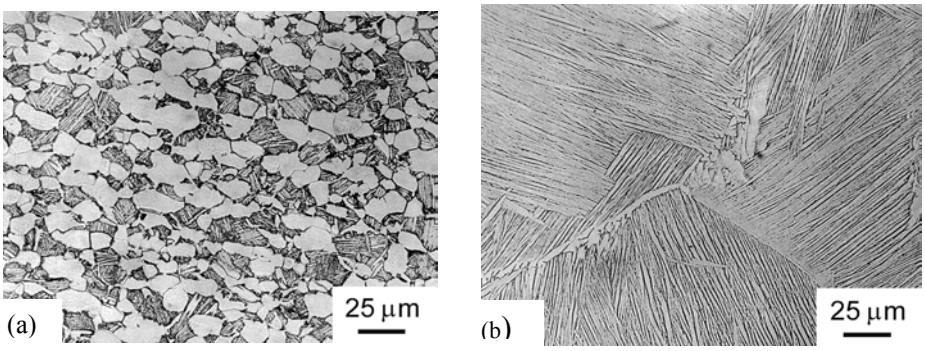

Fig. 1: Optical micrographs of the (a) bimodal and (b) lamellar microstructures of Ti-6Al-4V.

Table I: Uniaxial Tensile and Toughness Properties of Ti-6Al-4V

Microstructure	Yield Strength (MPa)	Ultimate Tensile Strength (MPa)	Reduction in Area (%)	Fracture Toughness K_{Ic} (MPa√m)
Bimodal	930	978	45	64
Lamellar	975	1055	10	100

Large (>4 mm) fatigue threshold testing was performed in four-point bending, using 6 mm thick samples with inner and outer spans of 12.7 and 25.4 mm, respectively. Pure mode I and mixed-mode tests were conducted using, respectively, symmetric (SFPB) and asymmetric (AFPB) four-point bending, with the ΔK_I and ΔK_{II} values computed from recent stress-intensity solutions [10]. Precracking was conducted in ambient air in near-identical fashion for all large and short crack tests; fatigue cracks were grown from a 2 mm deep through-thickness notch using SFPB at a load ratio of 0.1. The final precrack length was 4.50 ± 0.25 mm at near-threshold ΔK_I values of 4.8 ± 0.5 MPa√m and 6.8 ± 0.5 MPa√m, respectively, for the bimodal and lamellar structures. Mode-mixities were varied from $\Delta K_{II}/\Delta K_I = 0$ (pure mode I) to ~7.1 (nearly pure mode II), representing a change in phase angle, $\beta = \tan^{-1}(\Delta K_{II}/\Delta K_I)$, from 0° to 82°. Load ratios were varied from $R = 0.1$ to 0.8. Tests were performed by cycling at a specific mode-mixity; if no crack growth was observed optically after $2x10^6$ cycles, either ΔK_I or ΔK_{II} was increased by ~0.25 MPa√m (with the other being increased accordingly to

maintain the mode-mixity) and the procedure repeated to obtain a "growth/no growth" condition bounding the threshold. The crack extension defining "growth" was taken to be the characteristic microstructural dimension (20 μm for the bimodal and 500 μm for the lamellar structure). The magnitude of the crack-tip shielding, used to compute the effective (near-tip) crack-driving force, was characterized using a recently developed compliance-based technique for both tensile opening and shear type loading; details are given elsewhere [7].

Mixed-mode threshold tests for the short cracks were measured using the same procedure as large cracks, except that the precrack wake was the carefully machined away to within ~200 μm of the crack-tip using a slow-speed diamond saw. The rationale for this procedure was to limit the effect of crack-tip shielding by minimizing the occurrence of any premature contact of the crack faces during unloading. Corresponding thresholds for microstructurally-small surface cracks were performed using an inclined-crack technique. Wide bend bars (16-25 mm wide, 5 mm thick) were machined in the L-T orientation. A "precrack" was naturally initiated at the stress of σ_{max} = 750 MPa using three-point bending. A bend bar was then cut from the original pre-cracked wide bar with the crack inclined at the desired angle (Fig. 2). The sample was then cycled at R = 0.1 in four-point bending until crack growth ensued. Due to highly deflected fatigue cracking, the inclined-crack technique could not be usefully employed for the lamellar structure.

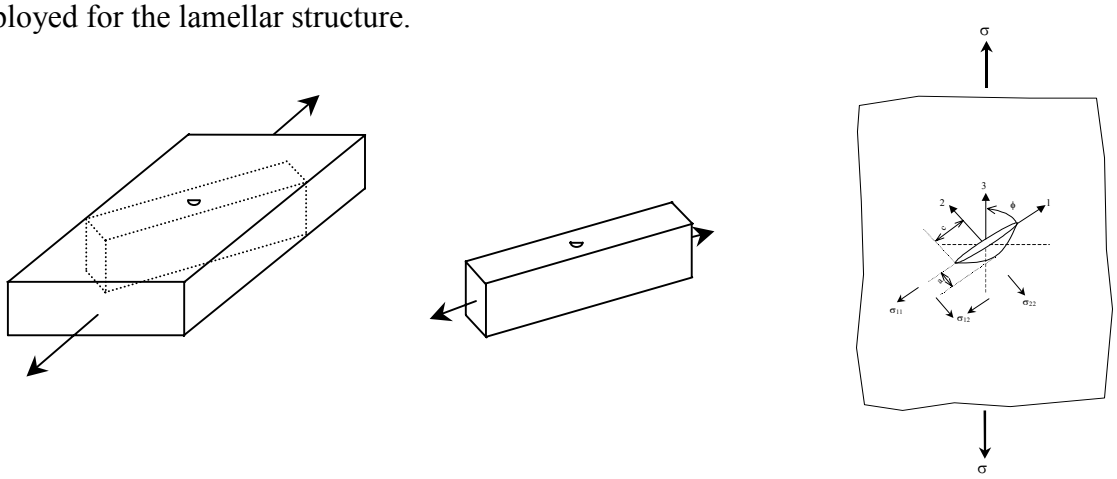

(a) **wide bend bar specimen** (b) **"inclined crack" specimen** (c) **small crack testing**

Fig. 2: Schematics showing (a,b) procedures used for obtaining the small "inclined crack" specimen from the wide bend bar, and (c) the configuration for such an inclined semi-elliptical surface crack.

For the small surface cracks, mode I stress intensities, K_I, were computed in terms of the remote uniform-tension σ_t and remote uniform outer-fiber bending σ_b stresses from [11]:

$$K_I = (\sigma_t + H\sigma_b) \sqrt{\pi \frac{a}{Q}} \; F\left(\frac{a}{t}, \frac{a}{c}, \frac{c}{b}, \theta\right), \tag{1}$$

where the geometrical factors H, Q and F are evaluated from the crack depth, a, the crack half-length, c, the specimen thickness, t, the specimen half-width, b, and the angular position along the crack front, θ [11]. Mode II components, K_{II}, were computed from [12]:

$$K_{II} = \chi \; \sigma_{12} \; \sqrt{\pi a} \;, \tag{2}$$

where χ is a numerical factor [12] and σ_{12} is the shear component of the loading.

RESULTS AND DISCUSSION

Large Cracks: Large crack thresholds for the bimodal and lamellar structures under mode I+II loading are shown in Fig. 3 in the form of mixed-mode threshold envelopes, where the mode II threshold stress-intensity range, $\Delta K_{II,TH}$, is plotted as a function of the corresponding mode I range, $\Delta K_{I,TH}$. Akin to behavior in most metallic alloys [e.g., 4-5], a reduction in the fatigue threshold values is clearly evident for both microstructures with increasing load ratio. The mode I threshold, $\Delta K_{I,TH}$, clearly decreases with increasing mode-mixity.

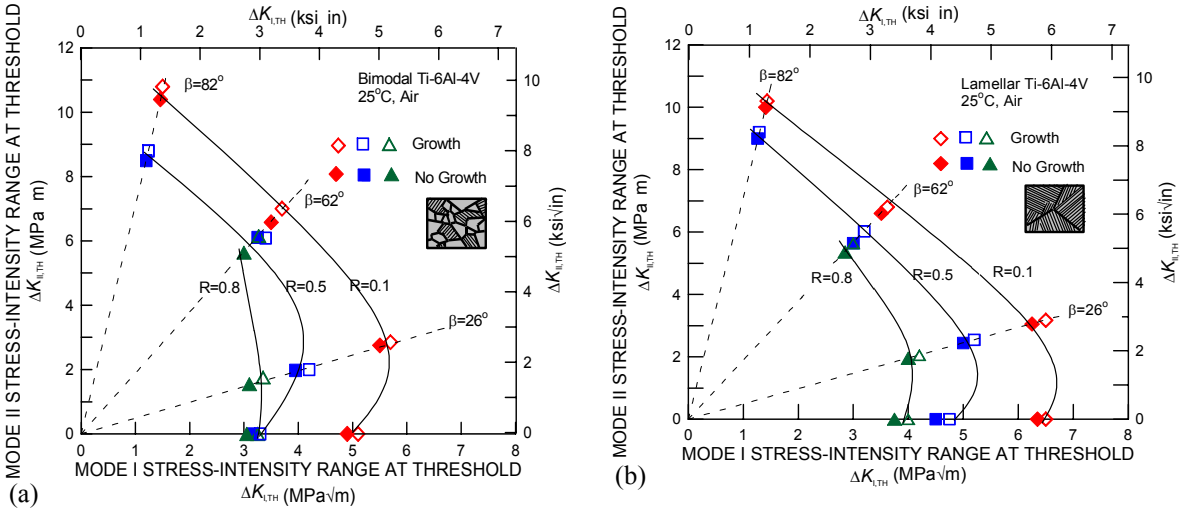

Fig. 3: Mixed-mode threshold envelopes for large (> 4 mm) through-thickness cracks in the (a) bimodal and (b) lamellar microstructures. Note that the lamellar structure shows superior resistance to crack propagation, particularly at the lower phase angles.

However, if the strain-energy release rate range, $\Delta G = (\Delta K_I^2 + \Delta K_{II}^2)/E'$, is used where $E' = E$ (Young's modulus) in plane stress and $E/(1-\nu^2)$ in plane strain (ν is Poisson's ratio), then there is a progressive increase in the mixed-mode ΔG_{TH} fatigue threshold with mode-mixity at all load ratios (Fig. 4). This can alternatively be expressed in terms of an equivalent stress-intensity range, $\Delta K_{eq,TH} = (\Delta G_{TH} E')^{1/2}$. Typical fractography is shown as insets in the Fig. 4.

From a perspective of HCF thresholds in Ti-6Al-4V, these results indicate that despite the presence of mixed-mode loading, the mode I threshold (for microstructurally-large cracks) defined in terms of ΔG represents a worst-case condition for the onset of crack growth under mode I+II loading. In general the lamellar structure exhibited higher threshold values and superior crack-growth resistance than the bimodal structure, which can be attributed to the large degree of crack-path deflection, bifurcation and secondary crack formation associated with crack extension in this structure (Fig. 5). This crack path results from a competition between the maximum crack-driving force and the weakest microstructural path. In the fine-scale bimodal structure, the crack-driving force is the dominant factor. For the coarse lamellar structure, microstructural factors play a much larger role, such that the crack does not deflect along the maximum tangential stress direction at the onset of the mixed-mode loading (Fig. 5).

All these factors result in substantially rougher fracture surfaces (Fig. 4 inset) in the lamellar microstructure, which *with large cracks* promotes both mode I crack closure, through

premature crack-surface asperity contact on unloading, and mode II crack-surface interference, through enhanced asperity rubbing and interlocking within the sliding crack faces. Measurements of the magnitude of such closure and surface interference, shown in Fig. 6, provide experimental confirmation of the more significant role of crack-tip shielding in the coarser lamellar structure; this is the main reason why this microstructure displays superior resistance to (large-crack) fatigue-crack propagation, with higher measured fatigue threshold values under both pure mode I and mixed-mode loading conditions.

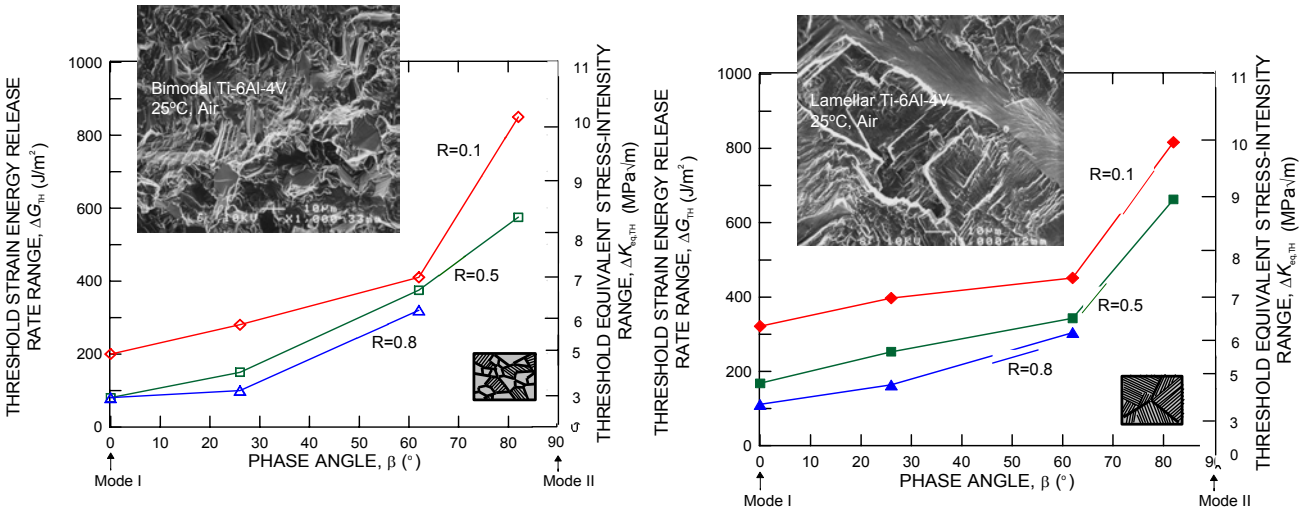

Fig. 4: Threshold strain-energy release rates ΔG_{TH} and equivalent stress-intensity ranges $\Delta K_{eq,TH}$, are plotted as a function of the phase angle β for large cracks in the (a) bimodal and (b) lamellar microstructures. The insets show typical fractography.

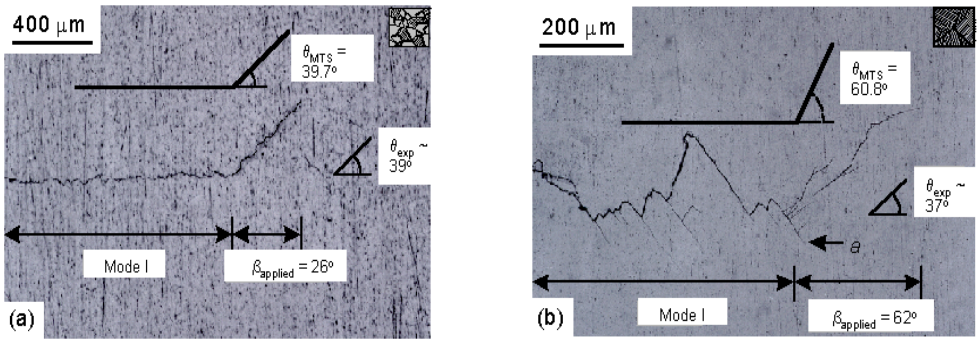

Fig. 5: Typical fatigue crack profiles are compared for the (a) bimodal (R = 0.8, β = 26°, ΔG_{TH} = 100 J/m^2) and (b) lamellar (R = 0.1, β = 62°, ΔG_{TH} = 450 J/m^2) microstructures, with the experimental and predicted crack deflection angles, θ_{exp} and θ_{MTS} (Maximum Tangential Stress), respectively.

In addition to the calculations shown above, an alternative method for calculating the threshold can be based on the presence of an infinitesimal kink along the observed crack direction. Assuming for the sake of simplicity that the kink (of length $b << a$, the crack length) represents an in-plane tilt through angle α to the precrack plane (Fig. 7 inset), then the local mode I and mode II stress intensities, Δk_1 and Δk_2, at the deflected crack tip will be given in terms of the stress intensities, ΔK_I and ΔK_{II}, for a main (pre)crack, by [13,14]:

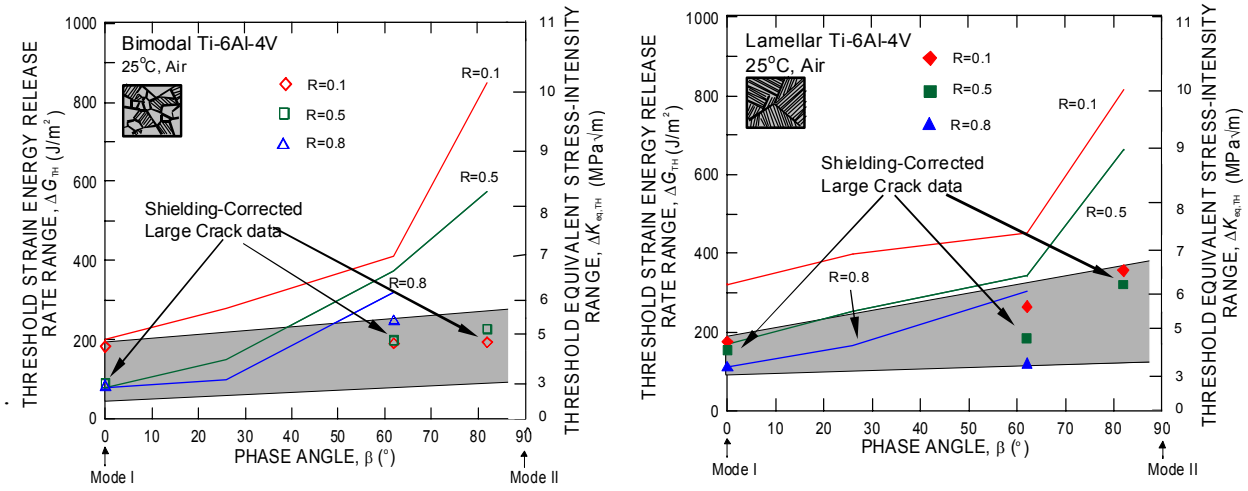

Fig. 6: The shielding corrected large crack thresholds for the bimodal and lamellar microstructures.

$$\Delta k_1(\alpha) = c_{11}\,\Delta K_{\rm I} + c_{12}\,\Delta K_{\rm II}\,; \quad \Delta k_2(\alpha) = c_{21}\,\Delta K_{\rm I} + c_{22}\,\Delta K_{\rm II}\ , \qquad (3)$$

where the coefficients c_{ij} are a sole function of α [13,14]. The mixed-mode $\Delta G'_{\rm TH}$ and $\Delta K'_{\rm eq,TH}$ thresholds can then be computed from:

$$\Delta G'_{\rm TH} = (\Delta k_{1,\rm TH}^2 + \Delta k_{2,\rm TH}^2)\,/\,E' \ \equiv \ (\Delta K'^2_{\rm eq,TH})\,/\,E' \ . \qquad (4)$$

Such thresholds are compared in Fig. 7 with those computed for unkinked large (Fig. 7a) and short (Fig. 7b) cracks. In general, the trend is to reduce the computed threshold values somewhat, except at very high phase angles. At $\beta = 26^{\rm o}$, however, the large crack $\Delta K_{\rm eq,TH}$ threshold is reduced by as much as 40%, this translates into a reduction in threshold $\Delta K_{\rm eq,TH}$ values by between 1 and 2 MPa√m. Effects are much less significant for the short cracks.

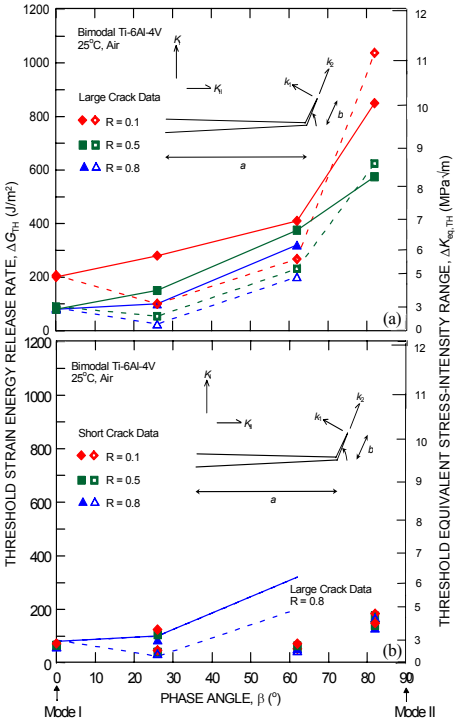

Fig. 7: Mixed-mode thresholds for (a) large cracks and (b) short cracks, calculated using the single-parameter characterization (solid lines, solid data points) and using the kink-based calculations (dotted lines, hollow data points).

Short cracks: Mixed-mode ΔG_{TH} thresholds for short (~200 μm) through-thickness cracks are plotted as a function of phase angle in Fig. 8; results are compared with the corresponding large crack thresholds. Due to the minimal role of crack-tip shielding associated with cracks of limited wake, measured short crack ΔG_{TH} thresholds were substantially lower than the corresponding large crack values, and furthermore were insensitive to mode-mixity and load ratio. The short-crack threshold values were observed to lie within the scatter band for shielding-corrected large cracks, again indicating that the limited effect of shielding for short cracks results in their lower threshold values. With respect to the role of microstructure, the distinction between the bimodal and lamellar structures in terms of the mixed-mode crack-growth resistance is substantially reduced for short cracks compared to that for large cracks. This again implies that the primary effect of microstructure on mixed-mode fatigue thresholds in Ti-6Al-4V arises through the mechanism of crack-tip shielding. Where the role of such shielding is restricted, as in the case of short cracks with limited wake, differences in fatigue resistance between the bimodal and lamellar structures become much less significant.

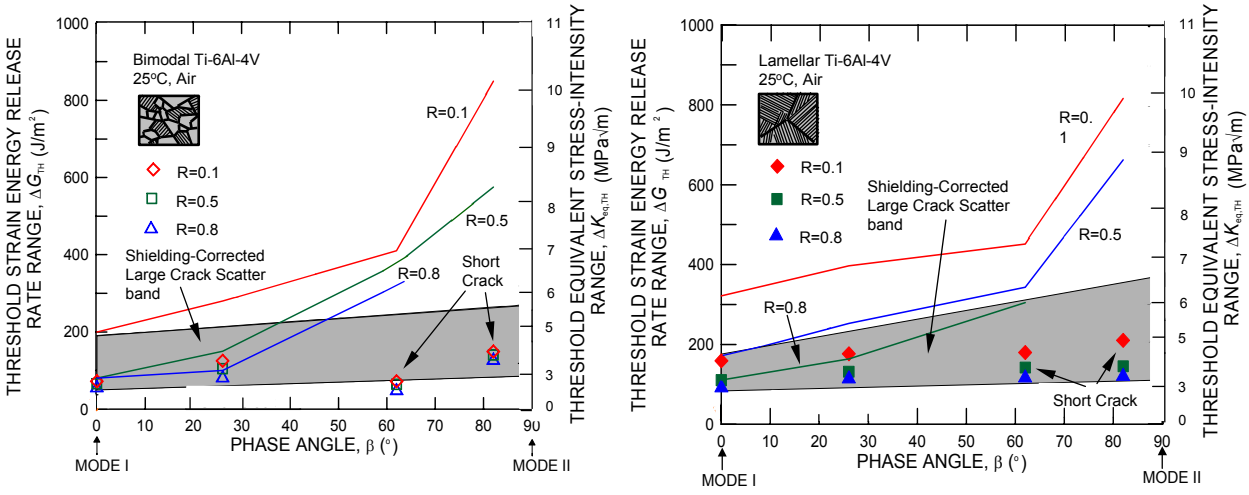

Fig. 8: Mixed-mode thresholds for large and short cracks in the (a) bimodal and (b) lamellar microstructures, showing how the small crack thresholds are comparable to the shielding-corrected large crack values.

Small cracks: Like short cracks, small cracks experience a minimal effect of crack-tip shielding due to their limited wake. Microstructurally, again it is clear that whereas the lamellar structure has superior large-crack threshold properties, this is not apparent in the presence of small cracks where the mode I thresholds are almost identical. Even the subsequent small-crack growth rates, shown as a function of ΔK_I in Fig. 9a from a parallel study on the effects of foreign-object damage on high-cycle fatigue in Ti-6Al-4V [15], reveal few differences in the behavior of the bimodal and lamellar microstructures, observations which can be related to the minimal role of crack-tip shielding with cracks of limited wake.

However, the behavior of the small surface crack is different from that of the short (and large) through-thickness crack in the manner in which it statistically "samples" the microstructure. In the present experiments where the small-crack dimensions were comparable with characteristic microstructural size-scales, their crack fronts cannot sample the "continuum" microstructure. For example, whereas the average short crack in the bimodal

microstructure would "sample" some 300 grains, the small crack merely "samples" one or two. Present results for the bimodal structure, at $R = 0.1$ only, are shown in Fig. 9b. Clearly, the additional effect of microstructural sampling is evident in these results in that the small crack thresholds can be seen to be lower than the corresponding values for short cracks and shielding-corrected large cracks. While the marked effect of crack size on the mixed-mode thresholds up to now has been attributed to a difference in the magnitude of the crack-tip shielding, the even lower mixed-mode thresholds for microstructurally-small cracks reflect this additional factor of the biased sampling of the "weak links" in the microstructure by the small flaw. Indeed, quantitatively, large crack mixed-mode ΔG_{TH} thresholds in the bimodal structure at high mode-mixities ($\Delta K_{II}/\Delta K_I = 7.1$) can be some ~50 to 90 times larger than such measured small-crack thresholds.

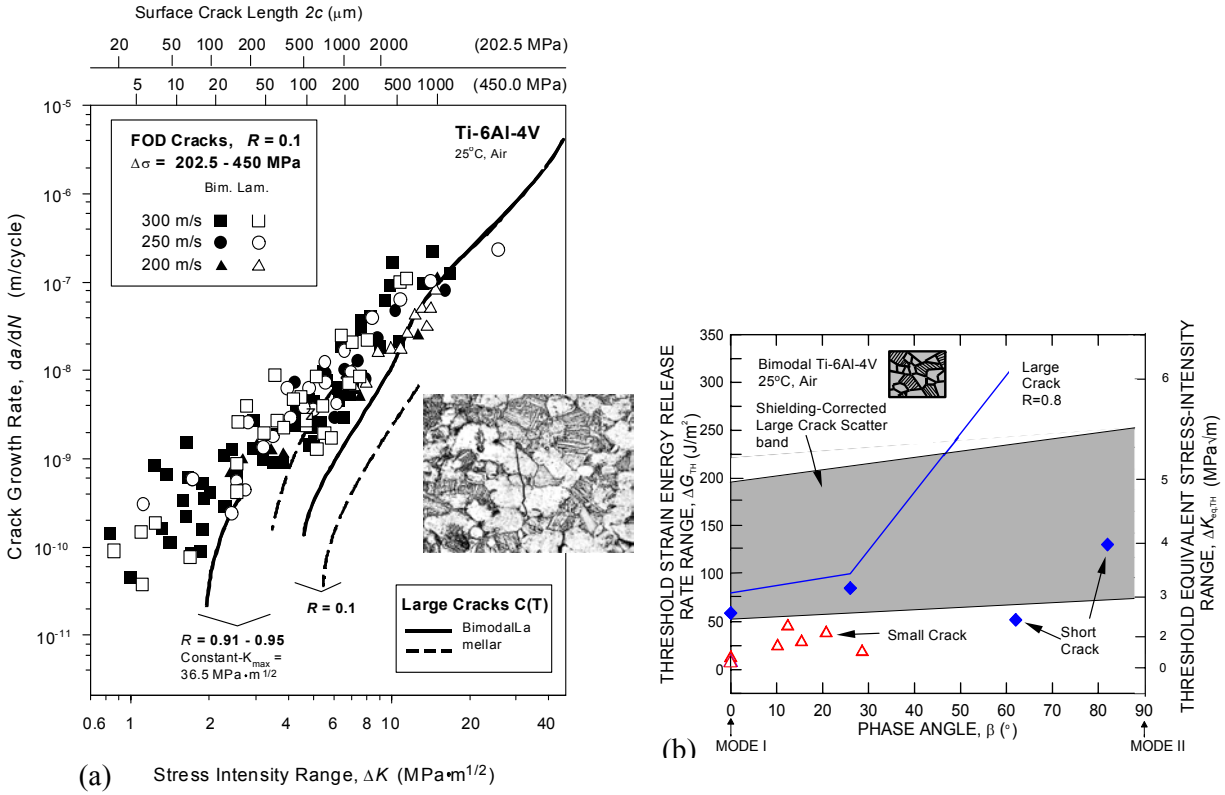

Fig. 9: (a) Pure mode I fatigue-crack propagation behavior for small cracks in bimodal and lamellar Ti-6Al-4V (after ref. [15]). The inset shows a typical small crack in the bimodal structure. (b) Mixed-mode thresholds for naturally-initiated small cracks in bimodal Ti-6Al-4V.

Concluding remarks: Finally, it is apparent that the near-elimination of the effect of mode-mixity on the large crack ΔG_{TH} thresholds when crack-tip shielding is accounted for (either by measurement or removal of the crack wake), strongly implies that the threshold behavior of fatigue cracks under mixed-mode loading is predominantly a mode I phenomenon. The principal influence of the applied shear loading appears to be in dictating the crack-path deflection, in conjunction with the near-tip microstructure in the coarser microstructures; once the crack path is set by the phase angle, the initial crack extension and hence the mixed-mode threshold are dictated by the effective crack-driving force, which is largely independent of

mode-mixity. The implications of this are that the mixed-mode fatigue threshold behavior is essentially identical to mode I behavior if the additional contributions to the crack-tip shielding that are induced due to a deflected crack path are carefully accounted for. Moreover, it further implies that the ΔG_{TH} threshold, measured under pure mode I loading, can be considered as a lower-bound.

CONCLUSIONS

Based on systematic investigation of the mixed-mode high-cycle fatigue threshold behavior of the bimodal (grain size ~20 μm) and lamellar microstructures (colony size ~500 μm) in a Ti-6Al-4V turbine engine alloy, the following conclusions can be made:

1. Both structures displayed a marked effect of mode-mixity and load ratio on the measured mixed-mode thresholds for through-thickness large (> 4 mm) cracks, with the lamellar structure showing generally higher thresholds. By characterizing the crack-driving force in terms of the strain-energy release rate, ΔG, the mode I threshold was found to represent the *worst-case* condition.
2. The marked effect of load ratio and mode-mixity was substantially reduced when the large-crack ΔG_{TH} thresholds were "corrected" for crack-tip shielding.
3 Mixed-mode ΔG_{TH} thresholds for through-thickness short cracks (~200 μm) were substantially lower than corresponding large-crack thresholds. Furthermore, such short crack thresholds were essentially insensitive to load ratio, mode-mixity and microstructure.
4. Mixed-mode ΔG_{TH} thresholds for microstructurally-small (< 50 μm) cracks in the bimodal microstructure were substantially lower than those for large cracks. In fact, large-crack thresholds at high mode-mixities ($\Delta K_{II}/\Delta K_I \sim 7.1$) were as much as ~50-90 times larger than such measured small-crack thresholds. This effect is believed to result from the limited role of crack-tip shielding and biased microstructural sampling by cracks of dimensions comparable with the characteristic microstructural size-scales.
5. The prime source of the influence of mixed-mode loading in dictating the value of the mixed-mode ΔG_{TH} threshold is considered to arise primarily from the trajectory of the precrack. Since microstructure can influence this trajectory, in general microstructural effects on mixed-mode thresholds result mainly from the role of crack-tip shielding that arises from such crack paths. Where crack sizes are small enough that such shielding cannot fully develop, the influence of microstructure on mixed-mode thresholds becomes minimal.

ACKNOWLEDGEMENTS

This work was supported by the U.S. Air Force Office of Scientific Research, Grant F49620-96-1-0478, under the auspices of the Multidisciplinary University Research Initiative on *High-Cycle Fatigue* to the University of California at Berkeley. Thanks are due to Dr. J. P. Campbell for this work on large-crack mixed-mode thresholds and to Drs. J. O. Peters and B. L. Boyce for many helpful discussions.

REFERENCES

1. Report of the AdHoc Committee on Air Force Aircraft Jet Engine Manufacturing and Production Processes (1992). United States Air Force Scientific Advisory Board, SAF/AQQS: the Pentagon, Washington, D.C.
2. R.B. Waterhouse and T.C. Lindley (1994). *Fretting Fatigue* (eds.). European Structural Integrity Society Publication No. 18, Mechanical Engineering Publications Ltd., London, U.K.
3. H. Gao, N. Alagok, M.W. Brown and K.J. Miller (1985). In: *Multiaxial Fatigue*, ASTM STP 853. ASTM, Philadelphia, PA, 184-202.
4. M.A Pustejovsky (1979). *Eng. Fract. Mech*., **11**, 9-15.
5. M.A. Pustejovsky (1979). *Eng. Fract. Mech*., **11**, 17-31.
6. J.P. Campbell and R.O. Ritchie (2000). *Eng. Fract. Mech.*, **67**, 209-27.
7. J.P. Campbell and R.O. Ritchie (2000). *Eng. Fract. Mech.*, **67**, 229-49.
8. J.P. Campbell and R.O. Ritchie (2001). *Metall. Mater. Trans. A*, **32A**, 497-503.
9. D. Eylon (1998). Summary of available information on the processing of the Ti-6Al-4V HCF/LCF program plates. Univ. of Dayton Report, Dayton, OH.
10. M.Y. He and J.W. Hutchinson (2000). *J. Appl. Mech.*, *Trans. ASME*, **67**, 207-09.
11. J.C. Newman and I.S. Raju (1981). *Eng. Fract. Mech.*, **15**, 185-92.
12. M.Y. He and J.W. Hutchinson (2000). *Eng. Fract. Mech.*, **65**, 1-14.
13. B.A. Bilby, G.E. Cardew and I.C. Howard (1978). In: Fracture 1977 (ed. D.M.R. Taplin); **3**:197-200.
14. B. Cotterell and J.R. Rice (1980). *Int. J. Fract.*, **16**:155-69.
15. J.O. Peters and R.O. Ritchie (2001). *Int. J. Fatigue*, **23**:1413-21.